



Coupling of the immersed boundary and Fourier pseudo-spectral methods applied to solve fluid–structure interaction problems

Andreia Aoyagui Nascimento¹ · Felipe Pamplona Mariano¹ · Aristeu da Silveira Neto² · Elie Luis Martínez Padilla²

Received: 6 May 2023 / Accepted: 6 February 2024 / Published online: 14 March 2024
© The Author(s) 2024

Abstract

The current manuscript addresses fluid–structure interaction (FSI) problems to the analysis of vortex-induced vibration (VIV), employing the methodology designated as IMERSPEC2D. The approach seamlessly integrates the Fourier pseudo-spectral method (FPSM) and the immersed boundary method (IBM) to solve the Navier–Stokes (NS) and continuity equations. Simultaneously, the effects of cylindrical structure, involving 1 and 2 degrees of freedom (d.o.f.) are simulated, by incorporating structural motion equations into NS via the IBM source term and implementing a two-way FSI algorithm. In the paper are presented the comparison of low and high-order temporal integration methods applied to solve the dynamic behavior of the structure and the dimensionless of the cylinder’s structural motion equations, resulting in an increase in computational time step from $1E(-9)$ to $1E(-3)$. Validation results to refined mesh simulations include the accurate representation of the lock-in phenomenon to simulations of 1 d.o.f. obtaining the range between reduced velocity 5.456 and 5.568 and the maximal amplitude is 0.352. Notably, the eight-shape pattern of the 2 d.o.f. cylinder displacement is obtained and the formation of C2S wake patterns is achieved, as presented by other authors. In conclusion, the dimensionless approach reduces computational time, while the high-order both of IMERSPEC methodology and time advancement integration to FSI improve the results of the cylinder’s motion and alters distinct vortex shedding patterns in fluid dynamics.

Keywords Fluid–structure interaction · Immersed boundary method · Fourier pseudo-spectral method · Flow over cylinder · Vortex-induced vibration

Technical Editor: Erick Franklin.

Andreia Aoyagui Nascimento, Felipe Pamplona Mariano, Aristeu da Silveira Neto and Elie Luis Martínez Padilla have contributed equally to this work.

✉ Felipe Pamplona Mariano
fpmariano@ufg.br

Andreia Aoyagui Nascimento
aanascimento@ufg.br

Aristeu da Silveira Neto
aristeus@ufu.br

Elie Luis Martínez Padilla
epadilla@ufu.br

¹ Laboratório de Engenharia Térmica e de Fluidos (LATEF), Escola de Engenharia Elétrica, Mecânica e de Computação (EMC), Universidade Federal de Goiás (UFG), Av. Esperança, s/n, Prédio B5, Goiânia, Goiás 74690-900, Brazil

² Laboratório de Mecânica dos Fluidos (MFLab), Faculdade de Engenharia Mecânica (FEMEC), Universidade Federal de Uberlândia (UFU), Av. João Naves de Ávila 2121, Bl. 5P, Uberlândia, Minas Gerais 38408-100, Brazil

1 Introduction

Fluid–structure interaction (FSI) gives rise to the phenomenon known as flow-induced vibration (FIV), which manifests in various scenarios involving fluid flows over different structures, whether rigid or flexible, including changes in orientation, bending and torsion. According to [48], FIV, in single phase flows, is classified into three types based on excitation characteristics: extraneously-induced excitation (EIE), instability-induced excitation (IIE) and motion-induced excitation (MIE). Each excitation can lead to four distinct phenomena: vortex-induced-vibration (VIV), vortex-induced-motion (VIM), wake-induced-vibration (WIV), galloping and flutter [14, 19, 42].

In the present work, the vortex-induced vibration (VIV) phenomenon is highlighted. The VIV occurs when, structures shed instabilities, forming a wake of vortical structures that tend to be similar regardless of structural geometry. When released, these instabilities generate pressure oscillations that induce effects on the structure, such as

displacements and deformations [5, 24] and where the shedding frequency of vortical structures closely aligns with the natural frequency of the body, a synchronization or lock-in phenomenon may ensue, leading to responses of significantly heightened amplitude. [63] categorized various regimes of vortex wake modes based both amplitude and frequency and introduced descriptive terminology for each mode. These modes include single vortices (S) and vortex pairs (P), leading to patterns like 2S, 2P and P+S, prominently observed near the fundamental lock-in region. One deduction from the [63] is that the phase change observed in classical forced vibration and free-vibration experiments is attributed to the transition from the 2S to the 2P mode, [61] and this phase transition has been observed in several free-vibration studies. Additional noteworthy aspects concerning the decomposition of force, the relevance of the paradigm flow of an elastically mounted cylinder to more complex systems, and the relationship between forced or free vibration, are presented in the work of [61].

For instance, in aerospace engineering, airflow over aircraft wings and control surfaces can induce fluttering. In civil engineering, buildings, chimneys and bridges must be designed to withstand vortex-induced vibrations (VIV). In ocean engineering, drilling and oil extraction pipelines (risers) are subjected to marine currents (VIV) [13, 27, 50, 62]. In wind engineering, interactions between flow and wind turbine blades and towers [29, 64], as well as the interaction of turbine wakes, modify the overall wind potential in wind farms (WIV). Offshore wind turbines also face FSI issues [19, 34], as they experience vibrations induced by both marine currents and waves. Power transmission towers and cables are also susceptible to flow-induced vibrations (galloping). In the examples described, flow-induced vibrations can lead to structural damage, [13, 51, 62], primarily through fatigue, often causing failures at anchoring and attachment points, and in some cases, structures may resonate, resulting in catastrophic damage. Hence, it is imperative to employ measures aimed at mitigating the adverse effects of VIV [20, 37, 63]

On the other hand, research is being conducted on devices that minimize these vibrations [49, 65] and, more importantly, harness FIV to generate electrical energy. Examples include the VIVACE (Vortex-Induced Vibrations for Aquatic Clean Energy) by Bernitsas et al. [4], capable of producing electricity from structural vibrations induced by water currents, and the vortice bladeless wind turbines [15, 17], equipped with specific linear electric generators that convert structural vibrations caused by the wind into electrical energy.

In the present paper simulations of free flows over circular cross-section cylinders anchored by springs are conducted, since they are widely used for validation of mathematical models and computational codes applied with

different computational fluid dynamics (CFD) techniques and physically representing scenarios like flows over power transmission cables, risers, bridge pillars, wind turbine towers and power transmission towers. Predicting both the frequency and amplitude of vibration is important for designing such equipment, aiming to minimize structural mass without compromising mechanical strength, ensuring a longer lifespan, and avoiding resonance issues. To address this, computational simulations of flows over cylinders anchored by one spring in transverse direction of flow (1 degree of freedom) and anchored by two springs in both the transverse and parallel directions of the flow (2 degrees of freedom) are presented. This problem is solved using the IMERSPEC methodology that combine the Fourier pseudo-spectral method (FPSM) with the immersed boundary method (IBM) to model fluid dynamics.

The study of the physical problem by means of CFD [18, 41] with high-order numerical accuracy methods provides numerical results with good accuracy, for example, high-order finite difference method and compact schemes [3, 23, 28, 30]. On the other hand, they have disadvantages such as high computational cost compared to conventional methods. The advent of spectral methods has made it possible to combine high accuracy with low computational cost [1, 38, 55], they are methods characterized by exponential convergence to the exact solution with increasing grid size.

Within the spectral methods group [9, 10, 40], the Fourier pseudo-spectral collocation method stands out among the others due to its high accuracy and its low computational cost, because the pressure term, in the Navier–Stokes equations for incompressible flows, can be replaced by the projection method, then the FPSM does not require the solution of a Poisson equation for the pressure field. Furthermore, the use of the fast Fourier transform (FFT) [7] has a computational cost of the order $O(N\log_2 N)$ compared to classical high-order methods of solving linear systems that have order of $O(N^2)$, where N is the number of mesh divisions, which results in an unusually fast time stepping procedure. Nonetheless, the disadvantage of the FPSM is the difficulty of working with complex geometries and non-periodic boundary conditions, in particular, can be only used to solve flow problems with periodic boundary conditions, like present in [33, 45, 46], which excludes its use in most general engineering configurations. In contrast, one of the most practical methods for working with complex and moving geometries is the immersed boundary method (IBM) [44, 52, 58].

IBM is a method that is characterized by imposing a source term in the Navier–Stokes equations, in order to virtually represent the boundary conditions within the flow [6, 22, 44, 54]. These methods have been used successfully in a variety of flow configurations within finite difference [52], finite volume methods [58, 59] and heat transfer problems [25, 39]. These methods have produced

good results with smaller computational costs than other more conventional methods using non-structured grids [26]. Despite the continuous improvement in the immersed boundary methods, the main drawback of these methods are their small accuracy near the boundaries of the immersed bodies [58, 59].

The coupling of immersed boundary and Fourier pseudo-spectral methods gives rise to a methodology IMERSPEC, which was presented in [31, 32]. The main objective this methodology is that it combines the advantages of each method and resolves some of their drawbacks. To overcome the periodic boundary condition requirement when using FFT, [31] propose dividing the computational domain into two, using IBM. Internally, the physical domain with boundary conditions imposed via IBM, and externally, the complementary domain for imposing periodic boundary conditions required by FFT. In this work, IBM is also utilized to model the structure of the cylinder immersed in the flow, enabling the representation of its structural movement. In [36] the authors presented the verification of the IMERSPEC using the multi-direct forcing [59], by using the manufactured solution proposed by Taylor and Green [56]. In aforementioned study, the authors note the high accuracy of the spectral method and address the influence when using the coupling with the IBM with two different interpolation and distribution functions.

To solve the FSI algorithm, a weak two-way approach is adopted. In a single time step, the fluid dynamics equations (Navier–Stokes and continuity equations) are solved first. Via IBM, the distributions of shear forces and pressure components acting on the cylinder’s surface are obtained, integrated and transferred to the structure’s center of mass (cylinder center). These distributions are then used as boundary conditions (excitation force) to solve the cylinder’s structural dynamics equations and determine its new position. Two key observations in the proposed algorithm include the adimensionalization of structural dynamics equations and the necessity of using a high-order convergence temporal integration method. In this work, the fourth-order Runge–Kutta method with six optimized steps, designed for low dispersion and dissipation by [2], is adopted. Both procedures allow the use of relatively large time steps, reducing computational processing time while maintaining accuracy in equation resolution.

The main objectives of this article are to present the developed algorithm for simulating fluid–structure interaction problems using the IMERSPEC methodology [31, 36], and validate the algorithm for the problem of vortex-induced vibration (VIV) generated in flows over cylinders anchored by springs, with 1 degree of freedom (d.o.f.) in the transverse direction and 2 d.o.f. in both transverse and flow directions. Demonstrating that it is possible to solve FSI problems with non-periodic boundary conditions using the FPSM.

Throughout this paper, the following are presented the evolution of the algorithm of FSI development to IMERSPEC methodology, for instance, comparing low and high-order temporal integration methods apply to solve dynamic of structure. Furthermore, the adimensionalization of the cylinder’s structural motion equations is employed, allowing for a significant increase in computational time steps. As results, the expected displacement amplitude and frequency are obtained for a wide range of reduced velocities. Notably, the displacement in the eight-shape pattern of the 2 d.o.f. cylinder is highlighted, along with the accurate representation of the lock-in phenomenon and the formation of several wake patterns such as the P+S mode.

2 Mathematical method

2.1 Fluid dynamics mathematical model with immersed boundary coupling

The flow is modeled with the mass balance equations, Eq. (1), and by the linear momentum balance equation, Eq. (2), considering a Newtonian fluid, incompressible flow, two-dimensional, no heat transfer, constant properties and no gravitational effects.

$$\frac{\partial u_j}{\partial x_j} = 0, \quad (1)$$

$$\frac{\partial u_j}{\partial t} + \frac{\partial u_j u_i}{\partial x_j} = -\frac{\partial p}{\partial x_i} + \nu \frac{\partial^2 u_i}{\partial x_j \partial x_j} + f_i, \quad (2)$$

where $\frac{\partial p}{\partial x_i} = \frac{1}{\rho_f} p' + gz$, p' is the static pressure in [N/m²]; u_i is the velocity in direction i in [m/s]; $f_i = \frac{f'_i}{\rho_f}$; f'_i is the source term in [N/m³]; ρ_f is the specific mass; ν is the kinematic viscosity in [m²/s]; x_i is the space component (x, y) in [m] and t is the time in [s], knowing that i and j are indices of the tensor notation.

The process of non-dimensionalization of Eqs. 1 and 2 is then conducted, employing the velocity magnitude at the inlet of the physical domain, U_∞ in [m/s], and the cylinder diameter, D , in [m], as parameters, then:

$$\frac{\partial u_j^*}{\partial x_j^*} = 0, \quad (3)$$

$$\frac{\partial u_j^*}{\partial t^*} + \frac{\partial u_j^* u_i^*}{\partial x_j^*} = -\frac{\partial p^*}{\partial x_i^*} + \frac{1}{Re} \frac{\partial^2 u_i^*}{\partial x_j^* \partial x_j^*} + f_i^*, \quad (4)$$

where u_i^* is the dimensionless velocity, u_i/U_∞ , p^* is the dimensionless pressure, $p/(U_\infty^2)$, f_i^* is the dimensionless

force field, $fD/(U_\infty)$, x_i^* is the dimensionless space component, x_i/D , and t^* is the dimensionless time, tU_∞/D , and Re is the Reynolds number, given by $Re = U_\infty D/\nu$, in the present paper the Reynolds number varies in the range of $80 \leq Re \leq 130$, indicating that all simulations are conducted laminar flow conditions [11].

The fluid/solid interface information was realized with IBM, where the Lagrangian domain (Γ) passes information to the Eulerian domain (Ω) by the source term, in Eq. (2) [31, 36]. The purpose of this term is to represent the boundary conditions of the complex geometry and the inlet velocity condition [21], as observed in Fig. 1.

In Fig. 1 is shown a sketch of the computational domain for studying the VIV problem. The circular-section cylinder is fixed by spring-damper system in the horizontal and vertical directions to the flow. The diameter of the circular cylinder is defined as D . The computational domain has the rectangular geometry with dimensions $35D$ in the horizontal direction and $17.5D$ in the cross flow direction. The physical domain is subdivided into three zones: buffer zone (BZ), forcing zone (FZ) and physical zone (PZ), which have lengths $L_{BZ} = 5D$, $L_{FZ} = 2D$ and $L_{PZ} = 25D$, respectively.

At L_{FZ} the inlet velocity profile is imposed by ($U_\infty = 1.0$ m/s) and ($V_\infty = 0.0$ m/s) and the flow in the vicinity of the circular cylinder (Fig. 1) promotes the existence of a resultant force, which is decomposed into two components acting on the immersed body: the lift force (transverse to the flow) and the drag force (in the direction of the flow).

Mathematically, the source term is represented by Eq. 5, [16, 36]:

$$f_i(\vec{x}, t) = \begin{cases} F_i(\vec{X}, t) & \text{if } \vec{x} = \vec{X} \\ 0 & \text{if } \vec{x} \neq \vec{X} \end{cases}, \quad (5)$$

where \vec{x} positions any point in the Eulerian domain (Ω), \vec{X} positions any point in the Lagrangian domain (Γ) and $F_i(\vec{X}, t)$ is the Lagrangian force defined in the domain Γ , [31, 36]. For modeling circular geometry, where the Lagrangian

points do not coincide with the Eulerian points, makes the distribution of the force $F_i(\vec{x}, t)$ over its surroundings. To this end, was made use of the distribution function, $D_h(\vec{x} - \vec{X})$, proposed by Peskin [43] (Eqs. 6 and 7) and was used the cubic function, W_c , Eq. (8), proposed by Tornberg and Engquist [57],

$$f_i(\vec{x}) = \sum_{\Gamma} D_h(\vec{x} - \vec{X}) F_i(\vec{X}) \Delta s^2, \quad (6)$$

$$D_h(\vec{x} - \vec{X}) = \frac{1}{h^2} W_c(r_x) W_c(r_y), \quad (7)$$

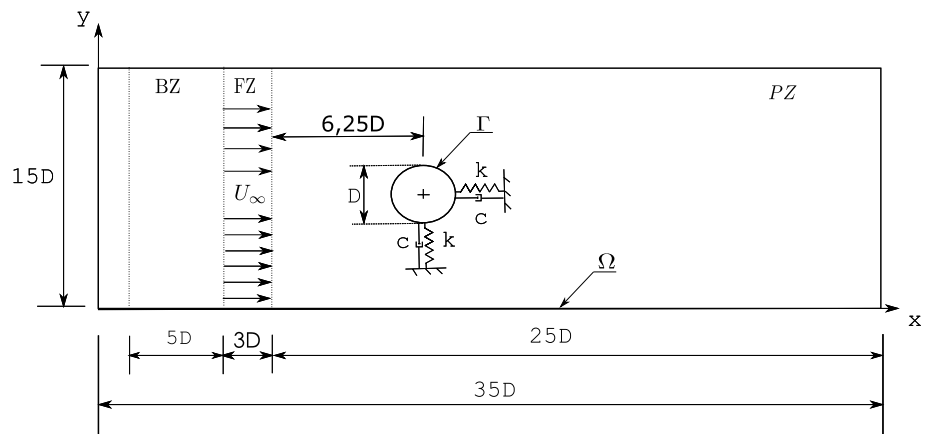
$$W_c(r) = \begin{cases} 1 - \frac{1}{2}|r| - |r|^2 + \frac{1}{2}|r|^3 & \text{if } 0 \leq |r| < 1 \\ 1 - \frac{1}{6}|r| + |r|^2 - \frac{1}{6}|r|^3 & \text{if } 1 \leq |r| < 2 \\ 0 & \text{if } 2 \leq |r| \end{cases}, \quad (8)$$

where $r_x = (x - X)/h$ and $r_y = (y - Y)/h$, being h the placement node spacing of the Eulerian domain when it is discretized, Δs is the discretized node spacing of the Lagrangian domain, and W_c , is the weight function. More details can be found in [52].

2.2 Structural mathematical model

The movement of the structure, Fig. 2, is due to the flow and the distance of the rigid body as it moves is obtained with the position vector, \vec{r}_{CB} , which is obtained by the difference of the positions between the inertial axis ($Bx'y'$) and the non-inertial axis (Cx_cy_c). In this manner, this position vector is related to the compression or tension of the spring in the system. The forces acting on the rigid body are shown in Fig. 2, where the equivalent spring force module components are, f^{eqsx} and f^{eqsy} , the equivalent fluid force module components f^{fx} and f^{fy} , and the equivalent damper force module components f^{eqdx} and f^{eqdy} .

Fig. 1 Sketch of the calculation domain employed in all simulations of the present paper



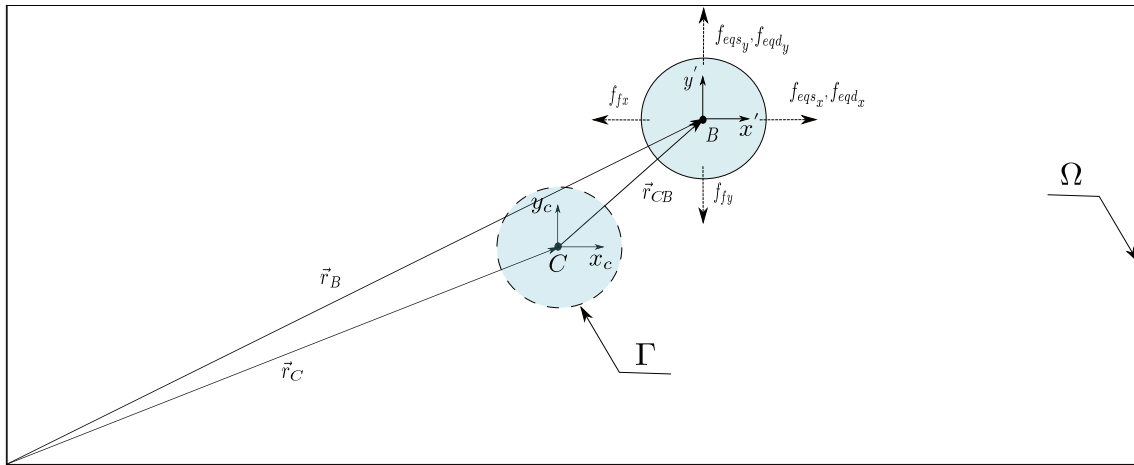


Fig. 2 Free-body diagram of the cylinder (Γ) inside the Eulerian domain (Ω)

The structural mathematical model was obtained with the Newton–Euler equation, given in indicial form by Eq. (9),

$$m_s \frac{d\vec{U}_i}{dt} = \vec{F}_i^{eqd} + \vec{F}_i^{eqs} + \vec{F}_i^f, \tag{9}$$

where m_s is the mass of the rigid body, \vec{U}_i is the translation velocity vector with respect to the structure centroid, \vec{F}_i^f is the flow force vector obtained by summing the forces acting at each Lagrangian point of the rigid body. Importantly, the fluid forces are calculated by summing the forces at the Immersed Boundary Method, specifically, by using the multi-direct forcing model [59], given by Eq. (10),

$$\vec{F}_f = - \sum_{i=1}^{NL} \vec{F}_i = - \sum_{i=1}^{NL} \rho \frac{\vec{U}_i^{CD}}{\Delta t} \Delta s \Delta x L, \tag{10}$$

where NL is the number of Lagrangian points on the immersed boundary, \vec{U}_i^{CD} is the difference vector of the Eulerian velocity and Lagrangian interpolated velocity and L is the unit length in the z direction of the cylinder.

From the free-body diagram and using the inertial axis ($Bx'y'$) and the non-inertial axis (Cx_cy_c) as a reference, the mathematical model of the structure’s motion is obtained, Fig. 2;

$$m_s \frac{d^2 \vec{r}_i^{CB}}{dt^2} = -c \frac{d\vec{r}_i^{CB}}{dt} - k\vec{r}_i^{CB} + \vec{F}_i^f. \tag{11}$$

Being F_i^f the sum of the forces of all Lagrangian points, which is transferred to the structure’s centroid, e.g.,

$$m_s \frac{d^2 \vec{r}_i^{CB}}{dt^2} + c \frac{d\vec{r}_i^{CB}}{dt} + k\vec{r}_i^{CB} = \frac{\vec{U}_i^{CD}}{\Delta t} \Delta s \Delta x L \rho, \tag{12}$$

where the term after the equal sign is the dynamic fluid force, F_D , obtained in Eq. (10) and Δs and Δx are the lengths required to calculate the fluid volume related to each Lagrangian point, noting that the length of the third dimension is unitary, because the problem is considered two-dimensional.

Using the studies of [12] and [13], the equation that models the motion of the structure was dimensionless by identifying the following no dimensional groups in Table 1 where f_n is the natural frequency in [Hz], k is the spring coefficient in [N/m] and c is the damper coefficient in [N.s/m]. The dimensionless of Eq. (11) starts by transforming the fluid force (drag and lift) coefficients:

$$m_s \frac{4}{\rho \pi D^2 L U_\infty^2} \frac{d^2 \vec{r}_i^{CB}}{dt^2} + c \frac{4}{\rho \pi D^2 L U_\infty} \frac{d\vec{r}_i^{CB}}{dt} + k \frac{4}{\rho \pi D^2 L U_\infty^2} \vec{r}_i^{CB} = F_i^f \frac{4}{\rho \pi D^2 L U_\infty^2}, \tag{13}$$

Looking at the first term of Eq. (13), and the parameters in Table 1,

Table 1 Dimensional groups, [12]

Description	Parameter	Dimensional groups
Time	t^*	$\frac{t u_\infty}{D}$
Displacement	\vec{r}_{CB}^*	$\frac{\vec{r}_{CB}}{D}$
Mass ratio	m^*	$\frac{4m_s}{\pi \rho D^2 L}$
Reduced velocity	U_r^*	$\frac{u_\infty}{f_n D}$
Structure ratio damping	ζ	$\frac{c}{2\sqrt{m_s k}}$
Reduced natural frequency	f_n^*	$\frac{f_n D}{u_\infty}$

$$\begin{aligned}
 m^* \frac{1}{U_\infty^2} \frac{DU_\infty^2}{D^2} \frac{d^2 \vec{r}_i^{CB*}}{dt^{2*}} + \frac{4c}{\rho \pi D^2 LU_\infty^2} \frac{DU_\infty}{D} \frac{d\vec{r}_i^{CB*}}{dt^*} \\
 + \frac{4kD}{\rho \pi D^2 LU_\infty^2} \vec{r}_i^{CB*} = \frac{2C_o}{\pi D}.
 \end{aligned}
 \tag{14}$$

where C_o represents the instantaneous lift coefficient C_l or drag coefficient C_d , due to the direction in which the flow is being analyzed. Inserting: $2m_s/2m_s$, to the second term of Eq. (14), and rearranging, it has obtained,

$$\begin{aligned}
 m^* \frac{d^2 \vec{r}_i^{CB*}}{dt^{2*}} + \frac{m^* c}{D 2m_s} \frac{2D^2 U_\infty}{U_\infty^2} \frac{d\vec{r}_i^{CB*}}{dt^*} \\
 + \frac{4kD^2}{\rho \pi D^2 LU_\infty^2} \vec{r}_i^{CB*} = \frac{2C_o}{\pi}.
 \end{aligned}
 \tag{15}$$

Knowing that $c/2m_s = \xi \omega_n$ and $k = \omega_n^2 m_s$, the Eq. (15), becomes:

$$\begin{aligned}
 m^* \frac{d^2 \vec{r}_i^{CB*}}{dt^{2*}} + \frac{2m^* (\xi \omega_n)}{U_\infty^2} \frac{d\vec{r}_i^{CB*}}{dt^*} \\
 + \frac{4(\omega_n^2 m_s)}{\rho \pi D^2 LU_\infty^2} \vec{r}_i^{CB*} = \frac{2C_o}{\pi},
 \end{aligned}
 \tag{16}$$

Looking at Table 1 and performing the substitutions of variables for dimensionless parameters and rearranging, the Eq. (16) can be presented as:

$$\begin{aligned}
 \left(\frac{d^2 \vec{r}_{CB}}{dt^2} \right)^* + \frac{4\pi \xi}{U_r} \left(\frac{d\vec{r}_{CB}}{dt} \right)^* \\
 + \left(\frac{2\pi}{U_r} \right)^2 \vec{r}_{CB}^* = \frac{2C_o}{\pi m^*}
 \end{aligned}
 \tag{17}$$

The equation’s dimensionless aspect of motion in the structure proved to be essential to achieve larger time step, Δt , in the fluid-structural coupling, used a time increment of 10^{-9} seconds for the time-advanced non dimensionless. However, a time increment of 10^{-3} seconds, was used, thus allowing more efficient simulations computationally.

3 Numerical method

The Eq. 2 using the Fourier pseudo-spectral method (FPSM) involves transforming the equation into spectral space. As a result, the formulation of the velocity field can be expressed as shown in Eq. 18.

$$\frac{\partial \hat{u}_j}{\partial t} + ik_j (\widehat{u_i * u_j}) = -ik_i \hat{P} + vk^2 \hat{u}_i + \hat{f}_i
 \tag{18}$$

where k is the wave number, \hat{u}_i is the velocity vector transformed, ι is the complex number $\sqrt{-1}$ and f_i is the source

term. The $(\widehat{u_i * u_j})$ is the non-linear term, that is solved by applying the FPSM [9, 35]. In the transformation of Eq. 1 define the plane π , which has zero divergences [31, 36].

$$ik_j \hat{u}_j = 0
 \tag{19}$$

The fluid–structure interaction in the IMERSPEC2D methodology was accomplished using the multi-direct forcing (MDF) approach. Thus, it is possible to construct the diagram of the newly developed computational algorithm, Fig. 3, where the subscript φ_{im} indicates that the variable has been projected onto the π plane.

4 Results and discussion

4.1 Cylinder anchored with a spring-damper system vertical

The computational simulations were set up according to references [13, 53], i.e., reduced velocities, $U_r = U_\infty/f_n D$, of $U_r^* = 4.45$ to $U_r^* = 7.238$; mass ratio $m^* = 149.1$; $f_n = 7.016$ Hz, cylinder diameter of $D = 0.0016$ m; structural damping ratio $\xi = 0.0012$ and time increment $\Delta t = 10^{-3}$ seconds. The simulations were performed using the fourth-order Runge–Kutta method optimized with six steps [2] to both fluid and structure dynamics, and the Eulerian domain shown in Fig. 1 as discretized with 512×256 collocation points.

In Fig. 4, the instantaneous vorticity fields are shown for different reduced velocities U_r^* . The flow passing through an immersed body notices its presence, and this is observed with the deceleration of the flow in vicinity of the solid structure and, by raising the velocity of flow a region of low pressure, downstream of the body is formed, sucking a portion of fluid, thus forming counter rotating structures, called von Kármán structures. The process of releasing a counter rotating structure provides the transmission of the dynamic fluid force to the spring-damper assembly, moving the cylinder in harmonic motion in the vertical direction. As the cylinder is anchored with different spring and damper conditions, the formed wakes exhibit patterns 2S distinct. Notably, for $U_r^* = 5.456$ and $U_r^* = 5.568$, the pairs of single vortical structures formed are closer together compared to the other instances. This is indicative that the cylinder motion dynamics are in synchronization with the vortex shedding dynamics, meaning the lock-in phenomenon is present.

It is also observed in Fig. 4 that vortical structures leaving the computational domain at $x/D = 35$ re-enter the Eulerian complementary domain at $x/D = 0.0$ due to the periodic boundary conditions imposed by the Fourier pseudo-spectral method (FPSM). Simultaneously, it is noted that these vortical structures are attenuated until their complete extinction,

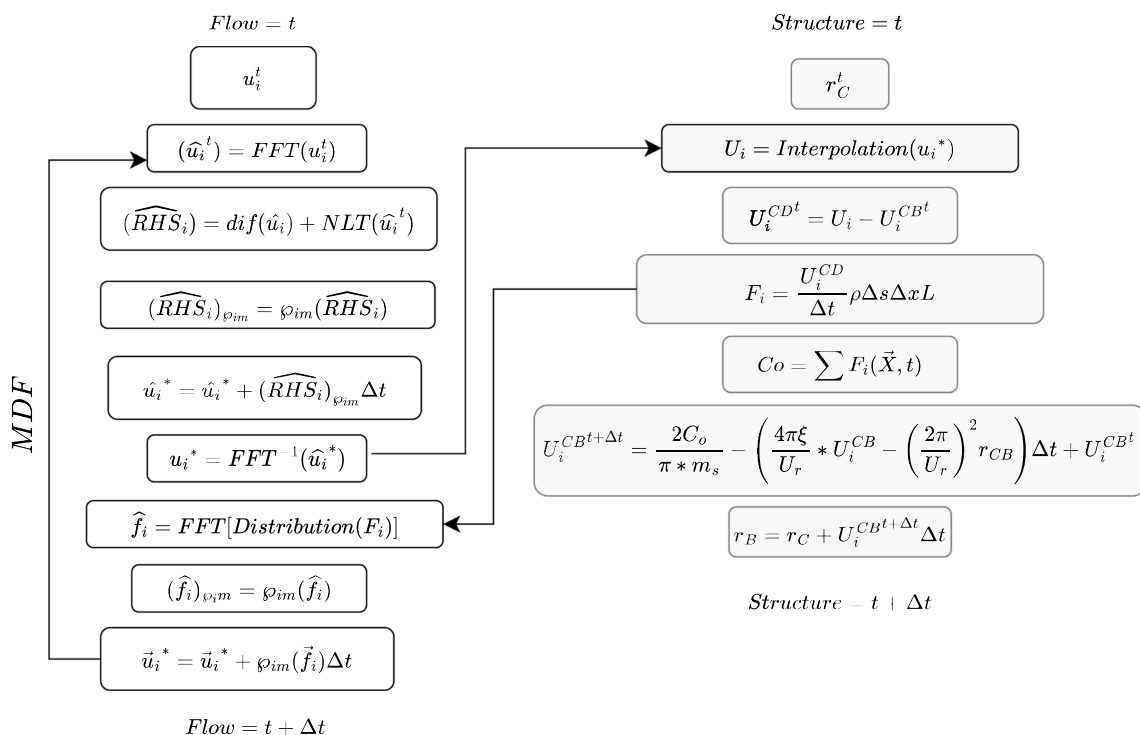


Fig. 3 Diagram of the newly developed computational algorithm

facilitated by the use of both buffer and forcing zones. The imposition of periodic boundary conditions is the main challenge when working with the FPSM.

In Fig. 5 are shown time evolution of the normalized transverse displacement of the vibrating cylinder in one vertical direction for $U_r^* = 4.45$ to $U_r^* = 6.68$. It is possible to observe, in the image for $U_r^* = 4.45$ that the vibration amplitude is small compared to the others. For $U_r^* = 5.456$ and $U_r^* = 5.568$, there is a significant increase in the vibration amplitude, it reaches a maximum value about $y/D = 0.352$, confirming the statements made about Fig. 4 that the lock-in phenomenon occurs within the range between $U_r^* = 5.456$ and $U_r^* = 5.568$, as also reported by Williamson and Rosko [63] and Chern et al. [12]. Additionally, for $U_r^* = 5.456$, the vibration beating phenomenon occurs, where the cylinder is subjected to excitation forces of frequencies that are close but different and the wave form of beating grows in each cycle and the vibration amplitude increases gradually. Finally, even for higher reduced velocities ($U_r^* = 5.84$, $U_r^* = 6.12$ and $U_r^* = 6.68$), the amplitude of structural motion is minimized, indicating the desynchronization of structural dynamics from the flow dynamics.

The maximal amplitude response is depicted in Fig. 6, of y/D versus the reduced velocity U_r^* . It exhibits significant similarity with that observed in both [12] and [13], except for $U_r^* = 5.568$, over which there is significant response lower than [12] and [13]. However, in terms of

validation of methodology, the number of collocation points is increased to 1024×512 , and the simulation is repeated with $U_r^* = 5.568$. Also is presented in Fig. 6 the red square that is the maximum amplitude response after refine meshed. Then it reached same result obtained by Chern et al. [12] and Dettmer and Peric [13]. This is the main advantage of the FPSM: high numerical convergence order. In other words, with the refinement of the computational mesh, there is a rapid (exponential) convergence to the correct response.

In Table 2 are shown the maximal amplitude and computational time of three different mesh have been simulated for $t^* = 68.75$ physical dimensionless time, and the computer configuration is Intel(R) Core i5-10400 CPU processor, clock speed 2.90 GHzx12. The results of maximum amplitude closely align with those presented by Chern et al. [12] and Dettmer and Peric [13] in mesh with 1024×512 collocation points. As described earlier, with mesh refinement, convergence of computational results is rapidly achieved using the FPSM. With respect to computational time, it is interesting to observe that by increasing the number of collocation points by a factor of 4, the computational time for the solution obtained by the FPSM increases approximately 5 times and 12 times. In contrast, for conventional methods, due to the solution of linear systems to solve the pressure field, an increase in N^2 is expected, where N is the number of collocation points [60]. The gain in computational time arises from three characteristics. The first is the immersed

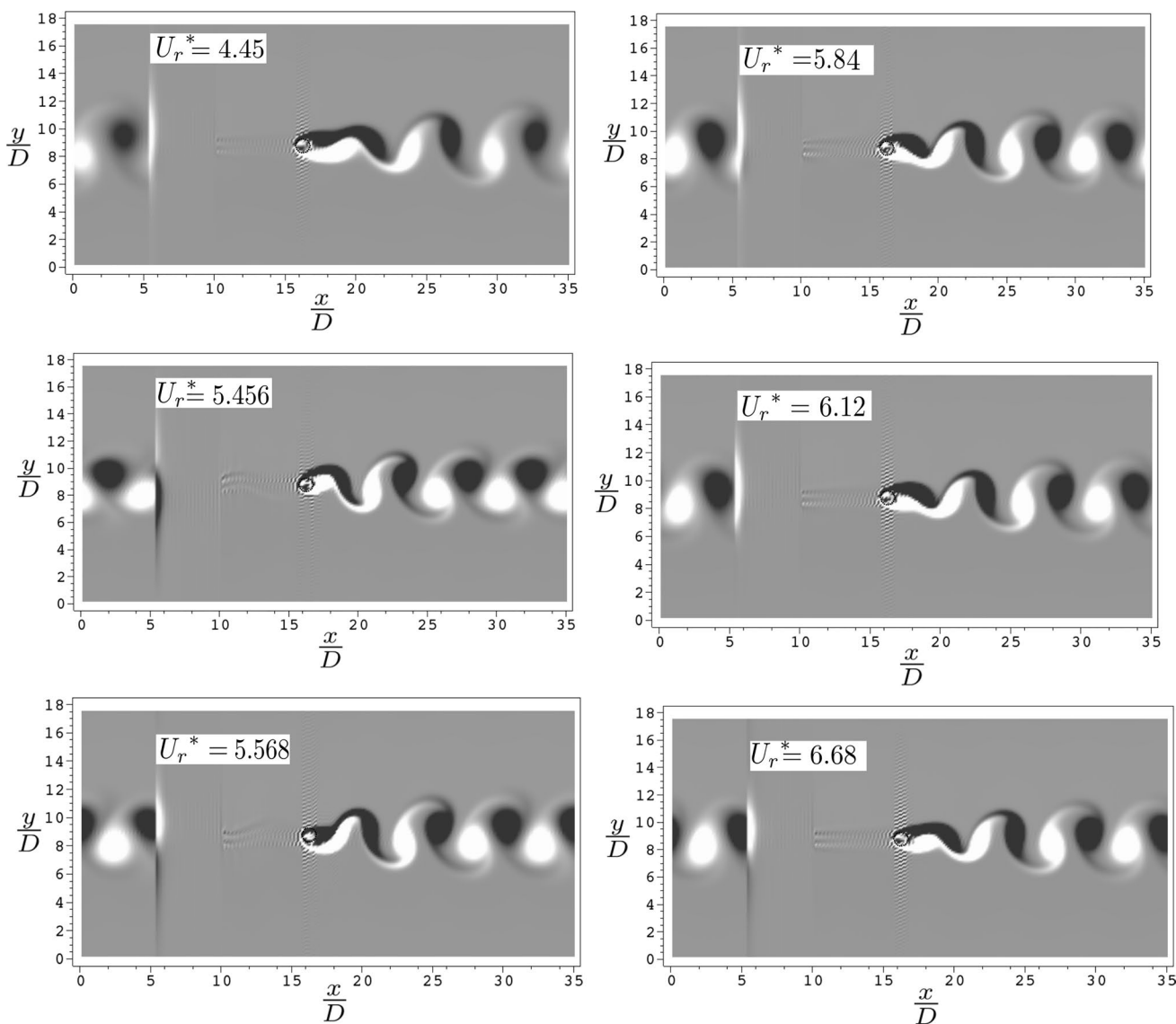


Fig. 4 Instantaneous vorticity fields in z direction (-20 [1/s], black color, to 20 [1/s], white color,) at $t^* = 1020$, to different reduced velocities U_r^* in flow over a cylinder with one degree of freedom in y direction

boundary method, which allows the use of a fixed and regular mesh for the Eulerian domain, even as the structure moves. Additionally, the non-dimensionalization of the structural motion equations allows an increase in the time step from 10^{-9} to 10^{-3} . Furthermore, despite the requirement for a complementary domain, the use of FFT in the discretization method proposed by the FPSM remains feasible.

In the Fig. 7 is presented the response of the Strouhal number, $St = Df_n/U_\infty$, which is normalized the structure natural frequency. The frequency ratio St/f_n^* coincide within the whole lock-in regions. It is another way to demonstrate that the lock-in phenomenon has been captured within the range between $U_r^* = 5.456$ and $U_r^* = 5.568$. In this case, there is agreement from both the structural

vibration frequency and the vortex shedding frequency in the flow dynamics. It can be observed that the results closely align with those obtained by Chern et al. [12] and Dettmer and Peric [13]. Furthermore, outside the lock-in range, there is also agreement with the theoretical results of [47].

The results presented throughout this section (Figs. 4, 5, 6, 7 and Table 2) indicate that the newly developed algorithm is feasible and consistent with the findings of [12] and [13], who conducted identical simulations with the same boundary conditions but using different computational methods. It is noteworthy that both studies also compared their results with other authors, including experimental works.

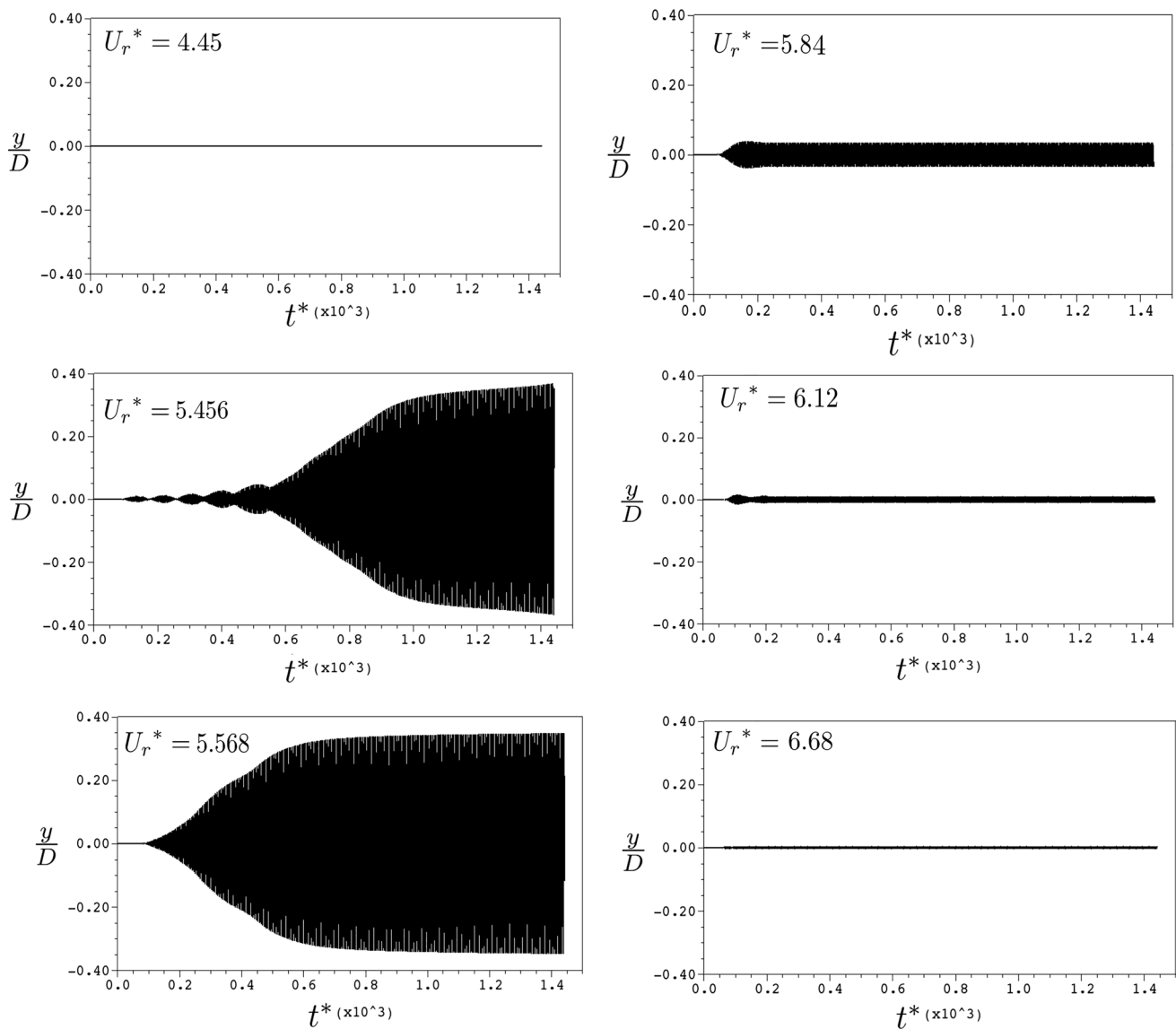


Fig. 5 Normalized displacement of the center of cylinder’s mass over time

4.2 Anchored cylinder with two spring-damper systems

The simulations are based on the studies of [12] and [53], the mass ratio between fluid and cylinder is $m^* = 10$, the damping ratio $\xi = 0$ and the reduced velocity was changed in the interval $4.0 \leq U_r^* \leq 8.5$, the natural frequency f_n , of both spring-damper systems are $f_{nx} = f_{ny} = 7.016$ Hz, the mesh has 512×256 collocation points and the time step $\Delta t = 10^{-4}$ s.

In Fig. 8, the instantaneous vorticity fields are shown for different reduced velocities U_r^* to simulations of an anchored cylinder with two spring-damper systems. In these simulations, the 2S pattern persists across the entire range of simulated reduced velocities ($4.2 \leq U_r^* \leq 8.5$). Specifically, at

$U_r^* = 4.5$, a new pattern emerges, known as C(2S), which is similar to the 2S mode, but with vortical structures coalescing in the wake downstream of the cylinder. These results are in accordance with the works of [12] and [53].

In Fig. 9, plots depicting the maximum amplitudes of cylinder center and the frequency ratio, both as a function of the reduced velocity U_r^* , are presented. These results are obtained in the present study and compared with the computational findings of [12] as well as the theoretical results of [47]. The results of Fig. 9a are approaching the [12] results, which are obtained using the finite volume method. It portrays the maximum value of the oscillation peaks of the structure are obtained after reaching a statistically stationary regime. It can be noted that the values obtained in Fig. 9b in the present study follow the same

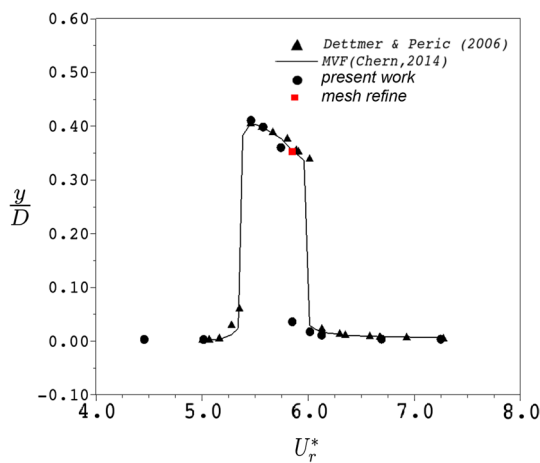


Fig. 6 Peak amplitude of the center of mass of the cylinder anchored by a spring

Table 2 Computational time and maximal amplitude to different meshes

Mesh	Computational time [s]	Maximum amplitude [y/D]
256 × 128	3637.03	0.0231
512 × 256	19658.70	0.035
1024 × 512	251132.80	0.352
[13]	–	0.364
[12]	–	0.354

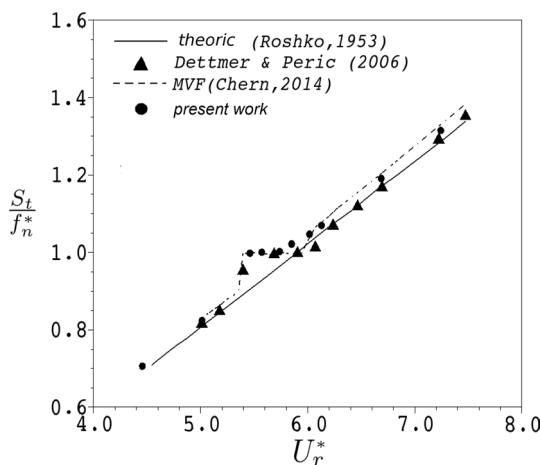


Fig. 7 Frequency ratio with increasing reduced velocity

trend as described by Roshko [47], Chern et al. [12] and Singh and Mittal [53]. Finally, it is possible to determine the lock-in range for flow simulations over cylinders with two degrees of freedom, defined between $4.4 < U_R^* < 7.4$.

Two computational experimentation was performed with two different advance time methods only for the structure movement, the first being the classical explicit Euler method (EEM) and the second being the Runge–Kutta fourth order six step method (RK46), which has low numerical diffusion and low dispersion proposed by [2]. The integral advance time to fluid dynamic is always RK46 method.

In Fig. 10 is shown the vorticity field of both methods, for $U_r^* = 4.9$. In Fig. 10 is highlighted the change in the pattern of the vortex shedding, in the simulations with RK46 the flow pattern is C(2S) and in the explicit Euler method the pattern is 2S. Comparing Fig. 10a and b, the change in flow behavior is evident when altering the temporal integration method of the structure motion. When using the EEM, structural motion is not satisfactorily obtained, resulting in 2S pattern that is different vortex generation from the expected. Performing the same simulation with RK46, proper structural motion is achieved, and as a consequence, fluid–structure interaction is correctly resolved. The vortex shedding pattern changes completely to C(2S).

To corroborate the image in Fig. 10, in Fig. 11 it can be seen the evolution of vertical amplitude response y/D of the cylinder center in time dimensionless. The simulation using the EEM shows the displacement is on the order of 10^{-3} and otherwise the RK46 simulation is larger displacement, nearly $y/D = 0.5$, as in the study of [12] and [53].

In Fig. 12, the XY-trajectory of the cylinder center over time is presented for the two tested temporal advancement methods. The motion described using the EEM method is on the order of $y/D = 10^{-3}$ and is entirely incorrect. On the other hand, the simulation result with RK46 is consistent with the expected behavior [12, 53], forming a eight-shape figure and achieving the correct amplitude of $y/D = 0.5$.

5 Conclusions

The motivations of the authors on the present article are to improve the Fourier pseudo-spectral method (FPSM), which is the method of high-order and low computational cost, but subject to periodic boundary conditions. Looking at this limitation, a fusion of the immersed boundary methodology to the classical FPSM has been done. Therefore, two degree of freedom vortex-induced vibration (VIV) of a spring-mounted circular cylinder has been simulated successfully using the multi-direct forcing in immersed boundary method.

The FPSM allows solving the equations for incompressible flows with high-order accuracy. Another advantage is the computational cost when compared to other high-order methods due to the pressure is decoupled from Navier–Stokes equations, [8–10], not requiring the use of the fractional step method. In addition, the present case of an

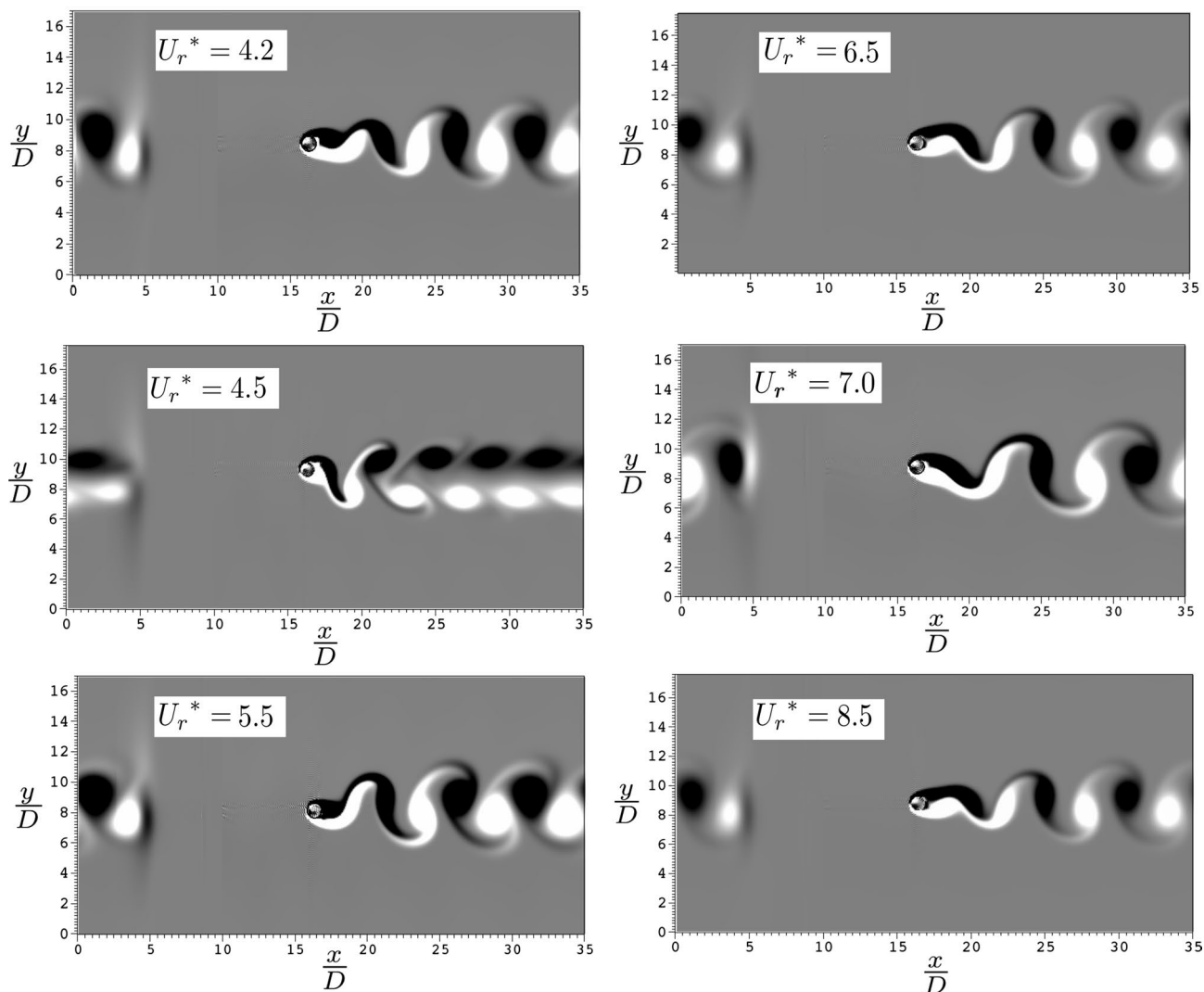


Fig. 8 Instantaneous vorticity fields in z direction (-20 [1/s], black color, to 20 [1/s], white color,) at $t^* = 1020$, to different reduced velocities U_r^* in flow over a cylinder with two degree of freedom in x and y directions

elastically mounted cylinder, the structure equation dimensionless is very important to reduce the time simulation from fluid–structure interaction.

The relationship between the reduced velocity and the vortex shedding mode is identified. By analyzing the amplitude vibration and reduced velocity, it is found that the *lock-in* region, which is the amplitude corresponding by greater peak amplitude, to 1 d.o.f. and 2 d.o.f.

In fluid–structure interaction simulations it is important to emphasize the advanced time method in both, fluid and rigid body motion, differential equations. It is necessary to use the high-order advanced time method; in the present paper was adopted the Runge–Kutta with low dissipation and low dispersion propose by [2]. Thereby, were allow to obtain the

correct flow pattern, the displacement of the cylinder center and the XY-trajectory.

Comparing the results of this article with the work of [12], which used the finite difference method (FDM) coupled with the IBM, the advantage of using IMERSPEC is evident. This is because the results presented by Chern et al. [12] were obtained with $dx = dy = 0.025$, while the mesh used in this study is $dx = dy = 0.136$, which is five times larger. In comparison to the work of [13], the authors used the finite element method with a mesh for the moving fluid, which increases the simulation time. Another notable point is that in this study, it is possible to visualize the vortical structures in detail.

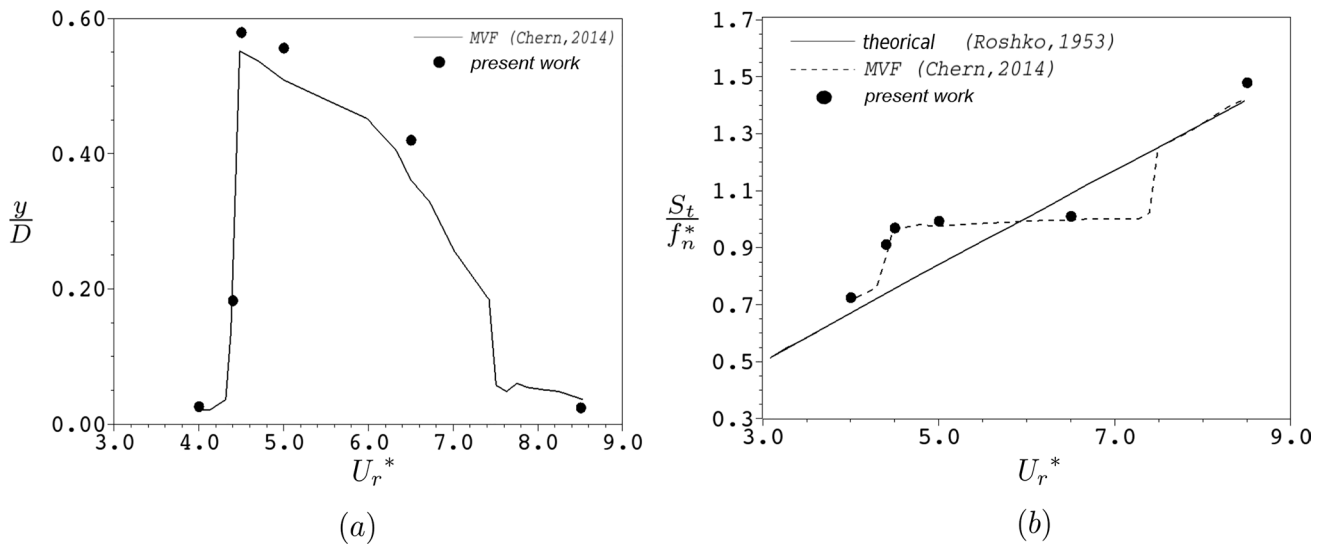


Fig. 9 **a** Amplitude response versus reduced velocity. **b** Ratio of the variation of frequencies with increasing reduced velocity

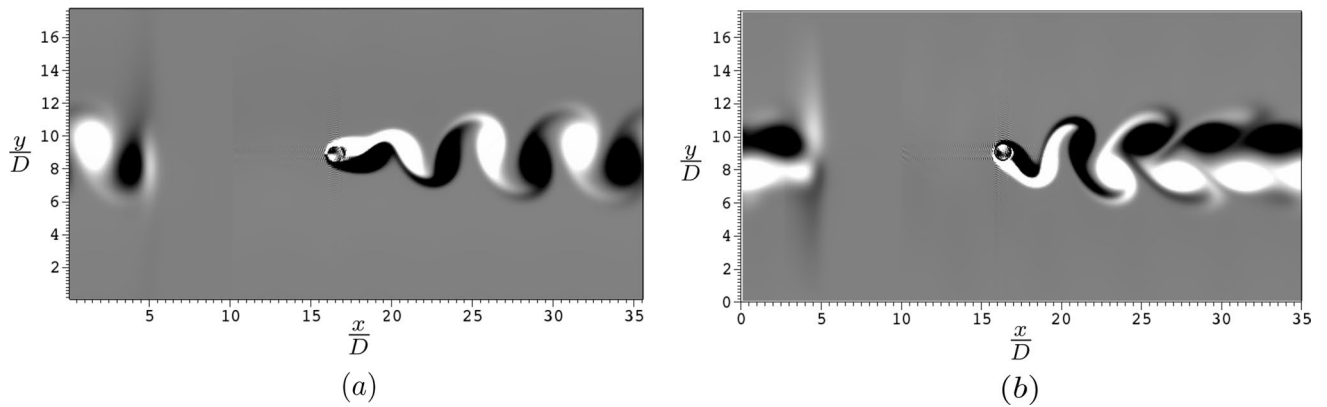


Fig. 10 Instantaneous vorticity fields in z direction (-20 [1/s], black color, to 20 [1/s], white color,) at $t^* = 1020$ for two degree of freedom flow and $U_r^* = 4.9$: **a** Explicit Euler method and **b** the Runge-Kutta fourth order six step method (RK46) [2]

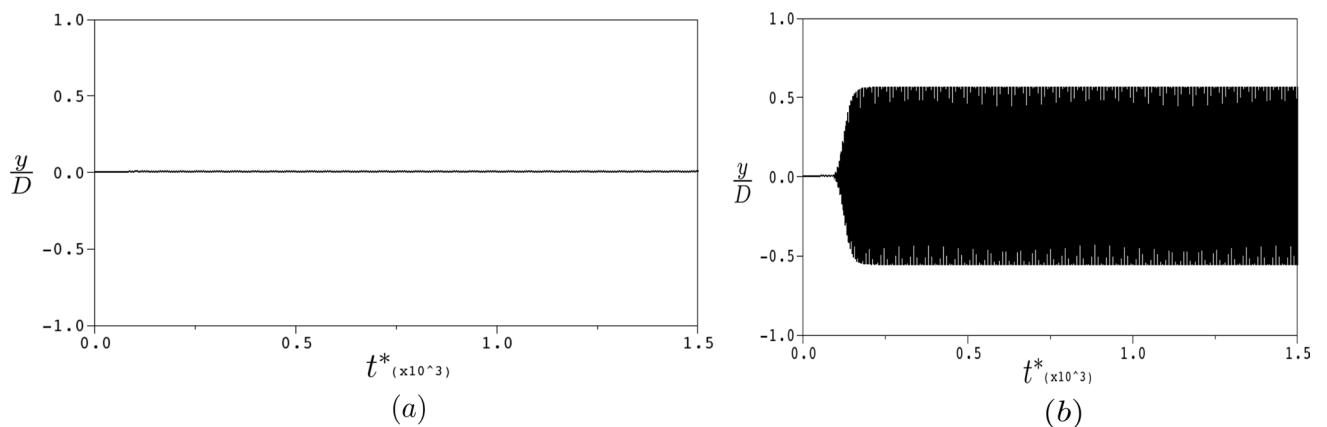


Fig. 11 Displacement as a function of time from the center of the cylinder: **a** Explicit Euler method, **b** Runge-Kutta fourth order six step method (RK46) [2]

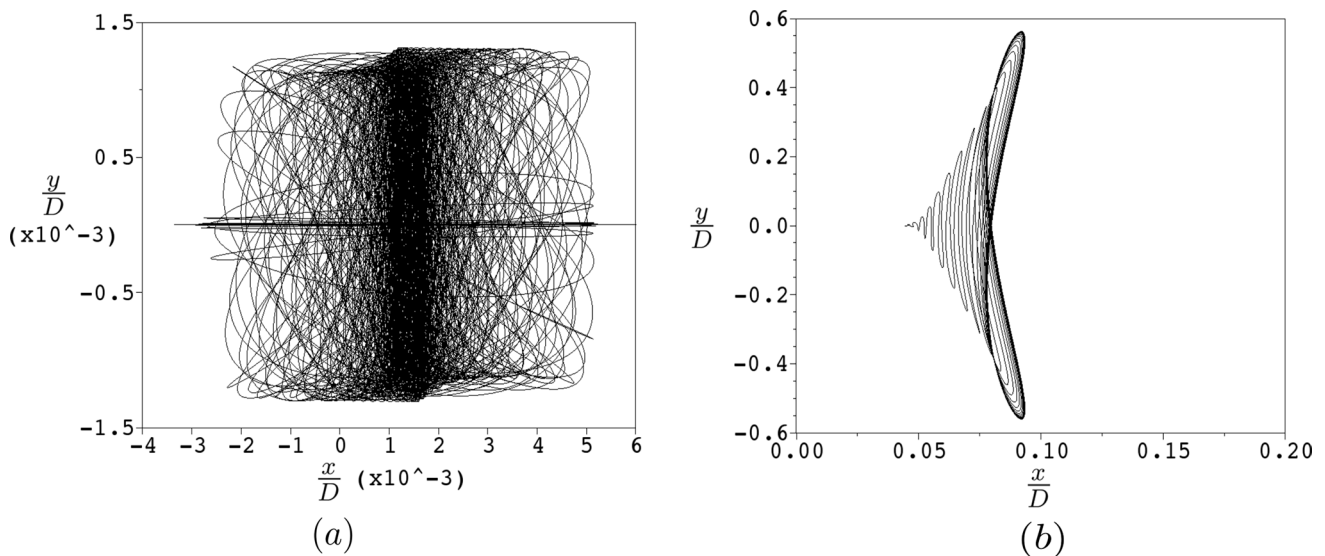


Fig. 12 XY-trajectories for two degree of freedom flow and $U_r^* = 4.9$: **a** explicit Euler method, **b** Runge–Kutta fourth order six step method (RK46) [2]

Acknowledgements Acknowledgment to Universidade Federal de Goiás (UFG), Universidade Federal de Uberlândia (UFU) and Graduate Program in Mechanical Engineering (PPGMEC-UFG) for administrative and technical support and FURNAS Centrais Elétricas and the “Programa de Pesquisa e Desenvolvimento Tecnológico” (P &D) of the ANEEL, Petrobras, CNPq, CAPES and FAPEG for the financial support.

Author contributions Conceptualization: A.A.N. and E.L.M.P.; methodology: A.A.N. and A.S.N. and F.P.M.; software: A.A.N. and F.P.M.; validation: A.A.N.; formal analysis: A.A.N. and A.S.N. and E.L.M.P.; resources: A.A.N. and F.P.M.; data curation: A.A.N. and A.S.N. and E.L.M.P.; writing—original draft preparation: A.A.N.; writing—review and editing: A.A.N. and A.S.N. and F.P.M. and E.L.M.P.; visualization: A.A.N.; supervision: A.A.N. and A.S.N. and E.L.M.P.; project administration: A.A.N. and A.S.N. and E.L.M.P.; funding acquisition: A.A.N. and F.P.M.

Funding The research leading to these results received funding from CNPq, CAPES, FAPEMIG, FAPEG, PETROBRAS and FURNAS Centrais Elétricas and the “Programa de Pesquisa e Desenvolvimento Tecnológico” (P&D) of the ANEEL.

Availability of data and materials The data and materials used in this study are available upon request from the corresponding author. We have followed best practices in data management and analysis to ensure the accuracy and validity of our findings.

Code availability The code used in the analysis is available upon request from the corresponding author. We have followed best practices in code development and management to ensure the accuracy and validity of our findings. The code has been thoroughly tested and validated, and any bugs or errors have been resolved.

Declarations

Conflict of interest The authors have no competing interests to declare that are relevant to the content of this article and have no relevant financial or nonfinancial interests to disclose.

Consent to participate All authors have worked to participate of the manuscript version.

Consent for publication All authors have read and agreed to the published version of the manuscript.

Ethical approval This study was conducted in accordance with ethical principles and guidelines set forth by the Universidade Federal de Goiás and Universidade Federal de Uberlândia. The research did not involve any human subjects or animals. We have followed best practices in data management and analysis to ensure the accuracy and validity of our findings.

Open Access This article is licensed under a Creative Commons Attribution 4.0 International License, which permits use, sharing, adaptation, distribution and reproduction in any medium or format, as long as you give appropriate credit to the original author(s) and the source, provide a link to the Creative Commons licence, and indicate if changes were made. The images or other third party material in this article are included in the article’s Creative Commons licence, unless indicated otherwise in a credit line to the material. If material is not included in the article’s Creative Commons licence and your intended use is not permitted by statutory regulation or exceeds the permitted use, you will need to obtain permission directly from the copyright holder. To view a copy of this licence, visit <http://creativecommons.org/licenses/by/4.0/>.

References

- Abd-Elhameed WM, Al-Harbi MS, Amin AK, et al (2023) Spectral treatment of high-order Emden–Fowler equations based on modified Chebyshev polynomials. *Axioms* 12(2). <https://www.mdpi.com/2075-1680/12/2/99>
- Allampalli V, Hixon R, Nallasamy M et al (2009) High-accuracy large-step explicit Runge–Kutta (*hale – rk*) schemes for computational aeroacoustics. *J Comput Phys* 228:3837–3850
- Avila R, Ramos E, Atluri SN (2009) The Chebyshev Tau spectral method for the solution of the linear stability equations for Rayleigh–Bernard convection with melting. *Comput Model Eng Sci* 51:73–92
- Bernitsas M, Ben-Simon Y, Raghavan K et al (2018) The VIVACE converter: model tests at high damping and Reynolds number around 10^5 . *J Offshore Mech Arct Eng* 131:1–13
- Blevins RD (1990) Flow-induced vibration, 2nd edn. Van Nostrand Reinhold, New York
- Borges JE, de Souza Lourenço MA, Padilla ELM et al (2021) A simplified model for fluid–structure interaction: a cylinder tethered by springs in a lid-driven cavity flow. *J Braz Soc Mech Sci Eng.* <https://doi.org/10.1007/s40430-021-03214-y>
- Briggs W, Herson V (1995) *The DFT*. SIAM, Philadelphia
- Canuto C, Quarteroni A, Hussaini MY et al (1988) *Spectral methods in fluid dynamics*, 2nd edn. Springer, New York
- Canuto C, Quarteroni A, Hussaini MY et al (2006) *Spectral methods-fundamentals in single domains*. Springer, New York
- Canuto C, Hussaini MY, Quarteroni A et al (2007) *Spectral methods: evolution to complex geometries and applications to fluid dynamics*. Springer, New York
- Carmo B, Meneghini J (2006) Numerical investigation of the flow around two circular cylinders in tandem. *J Fluids Struct* 22(6):979–988
- Chern MJ, Kuan YH, Nugroho G et al (2014) Direct-forcing immersed boundary modeling of vortex-induced vibration of a circular cylinder. *J Wind Eng Ind Aerodyn* 134:109–121
- Dettmer W, Peric D (2006) A computational framework for fluid-rigid body interaction: finite element formulation and applications. *Comput Methods Appl Mech Eng* 195:1633–1666
- Dilworth J, Ashby B, and Young P (2018) Fluid structure interaction simulation of Hood Flutter. In: Proceedings of the 15th international LS-DYNA users conference, detroit, livermore software technology corporation, pp 1–16. Available in <https://www.dynalook.com/conferences/15th-international-ls-dyna-conference>
- Elsayed AM, Farghaly MB (2022) Theoretical and numerical analysis of vortex bladeless wind turbines. *Wind Eng* 46(5):1408–1426. <https://doi.org/10.1177/0309524X221080468>
- Enriquez-Remigio S, Silveira-Neto A (2007) A new modeling of fluid–structure interaction problems through immersed boundary method/virtual physical model (IBM/VPM). In: Proceedings of the 19th brazilian congress of mechanical engineering, vol 1, pp 1–10. Available in <https://abcm.org.br/anais/cobem/2007/inicio.htm?query=remigio>
- Farsi M, Shariatzadeh M, Bijarchi M et al (2022) Low-speed wind energy harvesting from a vibrating cylinder and an obstacle cylinder by flow-induced vibration effect. *Int J Environ Sci Technol* 19(3):1261–1272. <https://doi.org/10.1007/s13762-021-03241-1>
- Ferziger J, Peric M (1996) *Computational methods for fluid dynamics*. Springer, New York
- Fujarra AL, Cenci F, Silva LS et al (2022) Effect of initial roll or pitch angles on the vortex-induced motions (VIM) of floating circular cylinders with a low aspect ratio. *Ocean Eng.* <https://doi.org/10.1016/j.oceaneng.2022.111574>
- Fujarra ALC, Leal AP, Carnier RM et al (2023) Validation of a low-cost IMU for flow-induced vibration tracking in offshore systems. *J Braz Soc Mech Sci Eng.* <https://doi.org/10.1007/s40430-023-04275-x>
- Goldstein D, Hadler R, Sirovich L (1993) Modeling a no-slip flow boundary with an external force field. *J Comput Phys* 105:354–366
- Iaccarino G, Verzicco R (2003) Immersed boundary technique for turbulent flow simulations. *Appl Mech Rev* 56(3):331–347
- Karniadakis G, Sherwin S (1999) *Spectral/HP element methods for CFD*. Oxford University Press, Oxford
- Khan N, Ibrahim Z, Khan MI et al (2018) VIV study of an elastically mounted cylinder having low mass-damping ratio using RANS model. *Int J Heat Mass Transf* 121:309–314
- Kim HJ, Choi (2004) An immersed-boundary finite-volume method for simulation of heat transfer in complex geometries. *KSME Int J* 18:1026–1035
- Kim J, Kim D, Choi H (2001) An immersed-boundary finite-volume method for simulation of flow in complex geometries. *J Comput Phys* 171(1):132–150. <https://doi.org/10.1006/jcph.2001.6778>
- Kiu K, Stappenbelt B, Thiagarajan K (2011) Effects of uniform surface roughness on vortex-induced vibration of towed vertical cylinders. *J Sound Vib* 330(20):4753–4763
- Lele S (1992) Compact finite difference schemes with spectral-like resolution. *J Comput Phys* 103:15–42
- Livanos D (2018) Investigation of vortex induced vibrations on wind turbine towers. Delft University of Technology, Delft, pp 1–86
- Lomtev I, Quillen CB, Karniadakis GE (1998) Spectral/HP methods for viscous compressible flows on unstructured 2D meshes. *J Comput Phys* 144:325–357
- Mariano F, Moreira LQ, Nascimento A et al (2022) An improved immersed boundary method by coupling of the multi-direct forcing and Fourier pseudo-spectral methods. *J Braz Soc Mech Sci Eng.* <https://doi.org/10.1007/s40430-022-03679-5>
- Mariano FP, Moreira LQ, Silveira-Neto A et al (2010) A new incompressible Navier–Stokes solver combining Fourier pseudo-spectral and immersed boundary methods. *Comput Model Eng Sci* 59:181–216
- Moreira L, Mariano FP, Silveira-Neto A (2011) The importance of adequate turbulence modeling in fluid flows. *Comput Model Eng Sci* 75(2):113–139
- Mougel J, Michelin S (2020) Flutter and resonances of a flag near a free surface. *J Fluids Struct* 96:103046. <https://doi.org/10.1016/j.jfluidstructs.2020.103046>
- Nascimento AA, Mariano FP, Silveria-Neto A et al (2014) A comparison of Fourier pseudospectral method and finite volume method used to solve the burgers equation. *J Braz Soc Mech Sci Eng* 36:737–742
- Nascimento AA, Mariano FP, Padilla ELM et al (2020) Comparison of the convergence rates between Fourier pseudospectral and finite volume method using Taylor-Green vortex problem. *J Braz Soc Mech Sci Eng* 42:1–10
- Nomura T, Hughes TJR (1992) An arbitrary Lagrangian–Eulerian finite element method for interaction of fluid and a rigid body. *Comput Methods Appl Mech Eng* 95:115–138
- Orszag SA (1970) Spectral methods for problems in complex geometries. *J Comput Phys* 37:70–92
- Pacheco-Vega A, Pacheco JR, Rodic T (2007) A general scheme for the boundary conditions in convective and diffusive heat transfer with immersed boundary methods. *J Heat Mass Transf* 129(11):1506–1516. <https://doi.org/10.1115/1.2764083>
- Pasciak JE (1980) Spectral and pseudo spectral methods for advection equations. *Math Comput* 35:1081–1092
- Patankar SV (1980) *Numerical heat transfer and fluid flow*. Taylor e Francis Book LTD, New York

42. Pesce CP, Orsino RMM, Silva LSP (2024) Nonlinear dynamics of variable mass oscillators. *Underst Complex Syst Part F* 1825:217–252. https://doi.org/10.1007/978-3-031-45101-0_8
43. Peskin C (1972) Flow patterns around heart valves: a numerical method. *J Comput Phys* 10:252–271. [https://doi.org/10.1016/0021-9991\(72\)90065-4](https://doi.org/10.1016/0021-9991(72)90065-4)
44. Peskin CS (2002) The immersed boundary method. *Acta Numer* 11:479–517. <https://doi.org/10.1017/S0962492902000077>
45. Pope S (2000) *Turbulent flows*. Cambridge University Press, New York
46. Roache PJ (1978) A pseudo-spectral FFT technique for non-periodic problems. *J Comput* 27:204–220
47. Roshko A (1953) On the development of turbulent wakes from vortex streets. Technical report, National Advisory Committee for Aeronautics - NACA TN 2913
48. Sharif M, Ghassemi H, He G et al (2023) A review of the flow-induced vibrations (FIV) in marine circular cylinder (MCC) fitted with various suppression devices. *Ocean Eng* 289:116261
49. Shi Z, Gao C, Dou Z et al (2023) Flow-induced vibration modeling of bluff bodies with data assimilation. *J Fluids Struct*. <https://doi.org/10.1016/j.jfluidstructs.2023.103866>
50. Shoghi R, Shiri H, Pesce C (2023) Dynamic curvature of a steel catenary riser on elastic seabed considering trench shoulder effects: an analytical model. *J Braz Soc Mech Sci Eng*. <https://doi.org/10.1007/s40430-023-04608-w>
51. Shyy W, Udaykumar HS, Rao MM et al (2007) *Computational fluid dynamics with moving boundary*. Dover Publications, Mineola
52. Lima e Silva AL, Silveira-Neto A, Damasceno J (2003) Numerical simulation of two dimensional flows over a circular cylinder using the immersed boundary method. *J Comput Phys* 189:351–370
53. Singh S, Mittal S (2005) Vortex-induced oscillations at low Reynolds numbers: hysteresis and vortex-shedding modes. *J Fluids Struct* 20:1085–1104
54. Sotiropoulos F, Yang X (2014) Immersed boundary methods for simulating fluid–structure interaction. *Prog Aerosp Sci* 65:1–21. <https://doi.org/10.1016/j.paerosci.2013.09.003>
55. Takei Y, Iwata Y (2022) Numerical scheme based on the implicit Runge–Kutta method and spectral method for calculating nonlinear hyperbolic evolution equations. *Axioms* 11(1). <https://www.mdpi.com/2075-1680/11/1/28>
56. Taylor GI, Green AE (1936) Mechanism of the production of small eddies from large ones. *Proc R Soc Lond Ser A Math Phys Sci* 158:499–521
57. Tornberg A, Engquist B (2004) Numerical approximations of singular source terms in differential equations. *J Comput Phys* 200:462–488
58. Uhlmann M (2005) An immersed boundary method with direct forcing for the simulation of particulate flows. *J Comput Phys* 209:448–476
59. Wang A, Fan J, Luo K (2008) Combined multi-direct forcing and immersed boundary method for simulating flows with moving particle. *Int J Multiph Flow* 34:283–302
60. Williams J, Sarofeen C, Shan H et al (2016) An accelerated iterative linear solver with GPUs for CFD calculations of unstructured grids. *Procedia Comput Sci* 80:1291–1300. <https://doi.org/10.1016/j.procs.2016.05.504>
61. Williamson C, Govardhan R (2008) A brief review of recent results in vortex-induced vibrations. *J Wind Eng Ind Aerodyn* 96(6):713–735. <https://doi.org/10.1016/j.jweia.2007.06.019>
62. Williamson CHK, Govardhan R (2004) Vortex-induced vibrations. *J Fluids Mech* 36:355–381
63. Williamson CHK, Rosko A (1988) Vortex formation in the wake of an oscillating cylinder. *J Fluids Struct* 2:355–381
64. Youssef M, el Moctar O, el Sheshtawy H et al (2022) Passive flow control of vortex-induced vibrations of a low mass ratio circular cylinder oscillating in two degrees-of-freedom. *Ocean Eng* 254:111–366
65. Zhao M (2023) A review of recent studies on the control of vortex-induced vibration of circular cylinders. *Ocean Eng* 285:115389. <https://doi.org/10.1016/j.oceaneng.2023.115389>

Publisher's Note Springer Nature remains neutral with regard to jurisdictional claims in published maps and institutional affiliations.